J. Fluid Mech. (1998), *vol.* 374, *pp.* 173–194. Printed in the United Kingdom

Viscous flow about a submerged circular cylinder induced by free-surface travelling waves

By B. YAN AND N. RILEY

School of Mathematics, University of East Anglia, Norwich, NR4 7TJ, UK

(Received 7 November 1997 and in revised form 8 May 1998)

Viscous flow about a circular cylinder that is submerged beneath free-surface travelling waves is considered. The wave amplitude is assumed small and results are presented for a wide range of Reynolds number. Particular attention is focused on the second-order time-averaged flow that manifests itself as a circulatory motion about the cylinder. The paper complements earlier work on this problem by Yan & Riley (1996) in the large Reynolds number, boundary-layer, regime and Riley & Yan (1996) in the inviscid flow limit, and makes a comparison with experimental work by Chaplin (1984) possible.

1. Introduction

In this paper we consider the two-dimensional flow induced in an incompressible, viscous fluid of infinite depth when monochromatic free-surface travelling waves propagate over a submerged circular cylinder whose generators are parallel to the wave crests. The amplitude of the incident waves is assumed to be small compared with the cylinder radius. Particular attention is paid to the second-order time-averaged flow that results in circulation about the cylinder.

The flow about a submerged circular cylinder, induced by small-amplitude free-surface travelling waves, has attracted attention over many years. The most recent interest is on account of the possible application to the flow about the submerged horizontal pontoons of tension-leg platforms. Dean (1948) and Ursell (1950) demonstrated that for an inviscid fluid of infinite depth the first-order reflection coefficient is zero. Vada (1987) continued this investigation to higher order, and his results suggested that the reflection coefficient at second order is also zero. This result was confirmed independently by Wu (1991) from a careful numerical investigation, and unequivocally by McIver & McIver (1990) by analytical means. Riley & Yan's (1996) numerical solutions are also in accord with this result. They complete the solution at second order by including the time-independent, or streaming, motion about the cylinder. This cannot be determined uniquely when the fluid is inviscid and in a subsequent paper, Yan & Riley (1996), they consider a fluid of very small viscosity. There is a boundary layer of double structure at the cylinder surface, and it is the relationship of this to the inviscid flow that uniquely determines the solution. This results in a non-zero time-averaged circulation about the cylinder. Recent experiments by Chaplin & Retzler (1997) confirm the presence of such circulation. The aim of the present paper is to extend the work of Yan & Riley (1996), who were concerned with an almost inviscid fluid, to finite values of the Reynolds number. This allows a comparison with some of the experimental results presented by Chaplin (1984) to be made.

The plan of the paper is as follows. In § 2 we briefly recapitulate the inviscid theory since the results from this will be used as approximate boundary conditions, in particular at the free surface. In § 3 we develop a viscous theory with a Reynolds number R_b based on a velocity ωa, where ω is the frequency of the incident waves, and cylinder radius a, that is $O(1)$. This is independent of $\epsilon = A/a$, where A is the wave amplitude, but solutions are obtained only for $\epsilon \ll 1$ in § 4. Section 5 is devoted to the same parameter range, but takes advantage of the small wave amplitude by developing the solution as a regular perturbation series in powers of ϵ. Both of these approaches encounter difficulties when R_b is large, on account of the thin Stokes shear-wave layer that develops on the cylinder surface. As a consequence for larger Reynolds numbers, specifically $R_b = O(\epsilon^{-2})$, we introduce a singular perturbation theory in § 6. In § 7 we discuss results. In particular we note the good agreement between the results of §§ 4 and 5, and conclude that the perturbation method is to be preferred on account of its computational efficiency. Results from the singular perturbation approach of § 6 provide a link between those of §§ 4, 5 and the almost inviscid, or infinite Reynolds number, theory of Yan & Riley (1996).

2. Inviscid theory

To prepare for the viscous calculations which follow we first, in this section, consider the flow that arises when two-dimensional waves at the free surface of an incompressible, inviscid fluid of infinite depth propagate over a submerged circular cylinder whose generators are parallel to the wave crest. If a is the radius of the cylinder, A the amplitude of the incident waves whose frequency is ω, and g the acceleration due to gravity, we define dimensionless quantities as follows:

$$\left.\begin{array}{llll} x = x'/a, & y = y'/a, & \epsilon = A/a, & h = H/a, \\ k = a\omega^2/g, & t = \omega t', & \eta = \eta'/a, & \phi = \phi'/\omega a^2. \end{array}\right\} \tag{2.1}$$

In (2.1) x', y' are Cartesian coordinates whose origin is at the centre of the cylinder with y' measured vertically upwards, t' is time, H is the depth of the centre of the cylinder below the undisturbed free surface and η' its elevation above it, ϕ' is the velocity potential of the flow, assumed irrotational. The non-dimensional geometry of the problem is shown in figure 1.

The flow under consideration is governed by Laplace's equation

$$\nabla^2 \phi = 0, \tag{2.2}$$

with boundary conditions at the free surface, derived from the kinematic and dynamic boundary conditions at the free surface respectively as

$$\frac{\partial \eta}{\partial t} + \frac{\partial \phi}{\partial x}\frac{\partial \eta}{\partial x} = \frac{\partial \phi}{\partial y}, \tag{2.3}$$

$$\eta(x,t) = -k\left[\frac{\partial \phi}{\partial t} + \frac{1}{2}\left\{\left(\frac{\partial \phi}{\partial x}\right)^2 + \left(\frac{\partial \phi}{\partial y}\right)^2\right\}\right]. \tag{2.4}$$

Under the assumption that $\epsilon \ll 1$ we now develop a solution in the classical form

$$\phi = \epsilon\phi^{(1)} + \epsilon^2\phi^{(2)} + ..., \tag{2.5}$$

$$\eta = \epsilon\eta^{(1)} + \epsilon^2\eta^{(2)} + ... \tag{2.6}$$

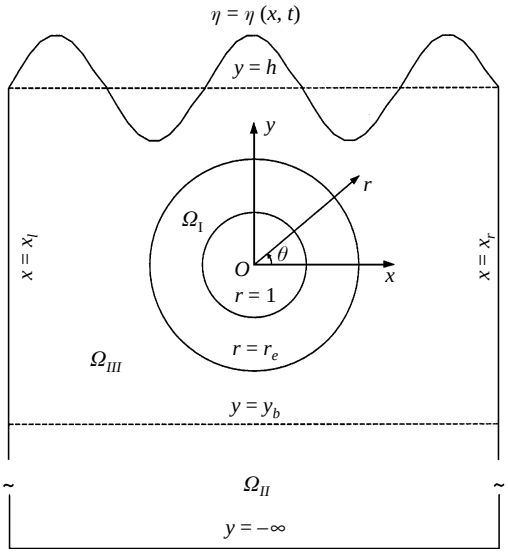

FIGURE 1. Non-dimensional geometry and solution domain.

If we substitute (2.5) into (2.2), then since the equation is linear each term $\phi^{(i)}$ satisfies Laplace's equation. Consider next the free-surface conditions (2.3) and (2.4). Not only are these nonlinear but are applied at a surface whose position is unknown *a priori*. We substitute the expansions (2.5) and (2.6) into (2.3) and (2.4), and simultaneously we transfer the boundary conditions from the exact free surface to its mean position $y = h$ by expanding the potential and its derivatives as Taylor series. Coefficients of like powers of ϵ then yield boundary conditions for the successive terms of our expansions. From (2.4) the terms $O(\epsilon)$, $O(\epsilon^2)$ give, respectively,

$$\left.\begin{aligned} \eta^{(1)} &= -k\left(\frac{\partial\phi^{(1)}}{\partial t}\right)_{y=h}, \\ \eta^{(2)} &= -k\left[\frac{\partial\phi^{(2)}}{\partial t} - k\frac{\partial\phi^{(1)}}{\partial t}\frac{\partial^2\phi^{(1)}}{\partial y\partial t} + \frac{1}{2}\left\{\left(\frac{\partial\phi^{(1)}}{\partial x}\right)^2 + \left(\frac{\partial\phi^{(1)}}{\partial y}\right)^2\right\}\right]_{y=h}. \end{aligned}\right\} \tag{2.7}$$

Carrying out the same procedure with (2.3), and using (2.7) to eliminate $\eta^{(1)}$, $\eta^{(2)}$ we have the conditions for $\phi^{(1)}$ and $\phi^{(2)}$ as

$$k\frac{\partial^2\phi^{(1)}}{\partial t^2} + \frac{\partial\phi^{(1)}}{\partial y} = 0, \tag{2.8}$$

$$k\frac{\partial^2\phi^{(2)}}{\partial t^2} + \frac{\partial\phi^{(2)}}{\partial y} = k\frac{\partial\phi^{(1)}}{\partial t}\left(k\frac{\partial^3\phi^{(1)}}{\partial y\partial t^2} + \frac{\partial^2\phi^{(1)}}{\partial y^2}\right) - 2k\left(\frac{\partial\phi^{(1)}}{\partial x}\frac{\partial^2\phi^{(1)}}{\partial x\partial t} + \frac{\partial\phi^{(1)}}{\partial y}\frac{\partial^2\phi^{(1)}}{\partial y\partial t}\right), \tag{2.9}$$

where all terms in (2.8) and (2.9) are evaluated at $y = h$.

We now write $\phi^{(1)}$, $\phi^{(2)}$ as

$$\phi^{(1)} = \overline{\phi}_{11}\cos t + \overline{\phi}_{12}\sin t = (\phi_{01} + \phi_{11})\cos t + (\phi_{02} + \phi_{12})\sin t, \tag{2.10}$$

$$\phi^{(2)} = \phi_{20} + \phi_{21}\cos 2t + \phi_{22}\sin 2t, \tag{2.11}$$

where $\phi_{ij} = \phi_{ij}(x, y)$. In equation (2.10) the incident wave is represented as

$$\phi_{01} \cos t + \phi_{02} \sin t = -\frac{1}{k} e^{k(y-h)} \cos(kx - t) = \phi_0 \tag{2.12}$$

say. On substituting (2.10) to (2.12) in (2.8) and (2.9) we derive the conditions at $y = h$ for ϕ_{ij}, together with other boundary conditions subject to which the following Laplace equations have to be solved:

$$\nabla^2 \phi_{ij} = 0, \quad i = 1, j = 1, 2; \quad i = 2, j = 0, 1, 2. \tag{2.13}$$

Details of the solution method may be found, for example, in Riley & Yan (1996) and will not be repeated here. If we now write the stream function ψ as

$$\begin{aligned} \psi &= \epsilon \psi^{(1)} + \epsilon^2 \psi^{(2)} + ... \\ &= \epsilon(\psi_{11} \cos t + \psi_{12} \sin t) + \epsilon^2(\psi_{20} + \psi_{21} \cos 2t + \psi_{22} \sin 2t) + ..., \end{aligned} \tag{2.14}$$

then each of these ψ_{ij} may be determined from $\overline{\phi}_{11}, \overline{\phi}_{12}, \phi_{20}, \phi_{21}$ and ϕ_{22} using the Cauchy–Riemann equations. We shall incorporate free-surface values of ψ_{ij}, so calculated, in our formulation of the viscous problem discussed below.

3. Viscous formulation

We consider a circular cylinder of radius a which is submerged in a fluid of viscosity μ under free-surface travelling waves

$$\eta = \eta(x, t), \tag{3.1}$$

where η is the elevation of the free surface above its mean position $y = h$. Under the assumption of $\epsilon \ll 1$ we neglect any terms higher than $O(\epsilon^2)$ in η, and the free surface elevation may then be approximated as

$$\eta = \epsilon \eta^{(1)} + \epsilon^2 \eta^{(2)}, \tag{3.2}$$

where $\eta^{(1)}$ and $\eta^{(2)}$ are defined in (2.7).

If we define non-dimensional quantities as in (2.1), take $U_0 = a\omega$ as the scale for velocity, then the two-dimensional governing equations for the viscous flow induced by the travelling waves can be written in terms of the stream function ψ and vorticity ζ as

$$\frac{\partial \zeta}{\partial t} + u \frac{\partial \zeta}{\partial x} + v \frac{\partial \zeta}{\partial y} = \frac{1}{R_b} \nabla_{xy}^2 \zeta, \tag{3.3}$$

$$\nabla_{xy}^2 \psi = -\zeta, \tag{3.4}$$

where

$$\nabla_{xy}^2 = \frac{\partial^2}{\partial x^2} + \frac{\partial^2}{\partial y^2}, \tag{3.5}$$

and

$$u = \frac{\partial \psi}{\partial y}, \qquad v = -\frac{\partial \psi}{\partial x}. \tag{3.6}$$

$R_b = a^2 \omega / \nu$ is the Reynolds number based on the frequency of the surface waves with ν the kinetic viscosity of the fluid.

If the plane-polar coordinate system (r, θ), with its origin located at the centre of the cylinder, is chosen then the governing equations in terms of ψ and ζ may be

written as

$$\frac{\partial \zeta}{\partial t} + \frac{1}{r}\left\{\frac{\partial}{\partial r}(ru_r\zeta) + \frac{\partial}{\partial \theta}(u_\theta \zeta)\right\} = \frac{1}{R_b}\nabla^2_{r\theta}\zeta, \tag{3.7}$$

$$\nabla^2_{r\theta}\psi = -\zeta, \tag{3.8}$$

where

$$\nabla^2_{r\theta} = \frac{\partial^2}{\partial r^2} + \frac{1}{r}\frac{\partial}{\partial r} + \frac{1}{r^2}\frac{\partial^2}{\partial \theta^2}, \tag{3.9}$$

and

$$u_r = \frac{1}{r}\frac{\partial \psi}{\partial \theta}, \qquad u_\theta = -\frac{\partial \psi}{\partial r}. \tag{3.10}$$

The fluid depth is again taken to be infinite. We assume that at large distances from the cylinder the flow is of potential type, and that the condition at the free surface is determined from the inviscid solution. The boundary conditions to be satisfied by (3.3)–(3.6), or (3.7)–(3.10) are then as follows:

$$\left.\begin{array}{llll} \dfrac{\partial \psi}{\partial r} = \dfrac{\partial \psi}{\partial \theta} = 0, & & \text{at} & r = 1, \\ \psi = \epsilon\psi^{(1)} + \epsilon^2\psi^{(2)}, & \zeta = 0, & \text{at} & y = h, \quad x_l \leqslant x \leqslant x_r, \\ \psi = \epsilon\psi^{(1)} + \epsilon^2\psi^{(2)}, & \zeta = 0, & \text{when} & x = x_l,\ x_r, \quad -\infty < y \leqslant h, \\ \psi = 0, & \zeta = 0, & \text{as} & y \to -\infty, \quad x_l \leqslant x \leqslant x_r, \end{array}\right\} \tag{3.11}$$

where x_l and x_r are the left and right boundaries of the solution domain of which the magnitudes are supposed to be large enough such that the numerical solution has sufficient accuracy, but usually smaller than those in § 2. The boundary conditions for ψ and ζ on the surface of the cylinder require care and we will return to this point in the next section. Two methods have been applied to solve the above viscous problem, namely a full numerical technique as described below and a perturbation method with numerical aid which will be described in §§ 5 and 6.

4. Numerical solution $R_b = O(1)$

The computational grid that we use for our numerical solutions is a hybrid one, in two parts. In the neighbourhood of the cylinder we use a grid based on plane-polar coordinates, elsewhere a grid based on Cartesian coordinates. Central differences are employed in our numerical scheme, and in the overlap domain flow variables are interpolated between the grids using techniques that maintain second-order accuracy. Since the solution domain extends to $y = -\infty$ it is convenient, for computational purposes, to introduce a new variable defined as

$$\xi = \xi(y) = \begin{cases} y, & \text{if } y \geqslant y_b \\ y_b + \alpha\left(1 - \dfrac{y_b}{y}\right), & \text{if } y < y_b. \end{cases} \tag{4.1}$$

In (4.1) y_b and α are constants to be chosen, with the requirement that $y_b < -r_e$ where r_e is the radial extent of the polar grid, so that $1 < r_e < h$. The solution domain is now divided into three sub-domains, see figure 1, as

$$\begin{array}{ll} \Omega_I : & 1 \leqslant r \leqslant r_e, \quad 0 \leqslant \theta < 2\pi, \\ \Omega_{II} : & x_l \leqslant x \leqslant x_r, \quad -\infty < y \leqslant y_b, \\ \Omega_{III} : & \{\Omega \setminus \{\Omega_I \cup \Omega_{II}\}\} \cup \{r_e - 5h_r \leqslant r \leqslant r_e, \quad 0 \leqslant \theta < 2\pi\}, \end{array}$$

where h_r is the mesh size in the radial direction. Note that, as defined, Ω_I and Ω_{III} share an overlap region in which interpolation of flow variables from one grid to the other can be carried out easily.

Following the transformation (4.1), the governing equations on the rectangular grid Ω_{II} and Ω_{III} may be written as

$$\frac{\partial \zeta}{\partial t} + u\frac{\partial \zeta}{\partial x} + \beta_1 v\frac{\partial \zeta}{\partial \xi} = \frac{1}{R_b}\nabla^2_{x\xi}\zeta, \tag{4.2}$$

$$\nabla^2_{x\xi}\psi = -\zeta, \tag{4.3}$$

where

$$\nabla^2_{x\xi} = \frac{\partial^2}{\partial x^2} + \beta_2\frac{\partial^2}{\partial \xi^2} + \beta_3\frac{\partial}{\partial \xi}, \tag{4.4}$$

and

$$u = \beta_1\frac{\partial \psi}{\partial \xi}, \qquad v = -\frac{\partial \psi}{\partial x}, \tag{4.5}$$

with

$$\beta_1 = \begin{cases} (\xi - \alpha - y_b)^2/(\alpha y_b), & \text{in } \Omega_{II}, \\ 1, & \text{in } \Omega_{III}, \end{cases} \tag{4.6}$$

$$\beta_2 = \beta_1^2, \tag{4.7}$$

$$\beta_3 = \begin{cases} 2(\xi - \alpha - y_b)^3/(\alpha y_b)^2, & \text{in } \Omega_{II}, \\ 0, & \text{in } \Omega_{III}. \end{cases} \tag{4.8}$$

In our numerical scheme the mesh sizes in the t-, x-, ξ-, r-, and θ-directions are denoted by h_t, h_x, h_ξ, h_r and h_θ respectively, with the number of mesh points in the negative x-, positive x-, negative ξ-, positive ξ-, r- and θ-directions denoted respectively by M_{xl}, M_{xr}, $N_{\xi s}$, $N_{\xi t}$, M_r and N_θ. The value of a typical dependent variable, say ψ, at $(x_i, \xi_j, t_l) = (ih_x, jh_\xi, lh_t)$ in Ω_{II} and Ω_{III} or $(r_i, \theta_j, t_l) = (1+ih_r, jh_\theta, lh_t)$ in Ω_I is denoted by $\psi_{i,j,l}$. A Crank–Nicolson scheme is employed for the vorticity transport equations (3.7) and (4.2), whilst in the Poisson equations (3.8) and (4.3) the finite-difference scheme is based on central differences. In the overlap region $\Omega_I \cap \Omega_{III}$, as the solution is carried from one mesh to the other, interpolation techniques are used that maintain second-order accuracy.

There are no restrictions on the parameter α in (4.1). Here we relate it to the values of of h_ξ and y_b. With h_ξ given we have $y_b = -N_{\xi b}h_\xi$, and we choose α such that $\xi(y_b - h_\xi) = y_b - h_\xi$. This choice ensures that in the original plane the mesh size in the y-direction is the same at points adjacent to $y = y_b$. This requires

$$\alpha\{1 - y_b/(y_b - h_\xi)\} + h_\xi = 0, \tag{4.9}$$

or

$$\alpha = y_b - h_\xi; \tag{4.10}$$

the total number of mesh points in the negative ξ-direction is $N_{\xi s} = 2N_{\xi b} + 1$.

In our stream function–vorticity formulation we require a boundary condition for ζ at the cylinder surface. Following Woods (1954) the vorticity on the boundary may be expressed in terms of its values at $r - 1 = h_r, 2h_r$, and the values of ψ at the first

three grid points, to the accuracy of our finite-difference scheme, as

$$\zeta_{0,j,l} = \frac{48\psi_{1,j,l} - 3\psi_{2,j,l} - 45\psi_{0,j,l} + 2h_r^2(4\zeta_{1,j,l} - \zeta_{2,j,l})}{4h_r^2(h_r - 3)}, \quad j = 1, 2, \ldots N_\theta, \quad l = 1, 2, \ldots . \tag{4.11}$$

There remains, to complete the formulation of our problem, the constant value of ψ, $\psi_{0,j,l}$, at the cylinder. Solutions may be obtained for any value of this constant; however, only one has any physical relevance, namely that which ensures the pressure is single valued. From the momentum equation in the θ-direction this condition is seen to require

$$I_{2\pi} \equiv -\frac{1}{R_b}\int_0^{2\pi}\left(\frac{\partial^3\psi}{\partial r^3} + \frac{\partial^2\psi}{\partial r^2}\right)_{r=1} \mathrm{d}\theta = \frac{1}{R_b}\int_0^{2\pi}\left(\frac{\partial\zeta}{\partial r}\right)_{r=1} \mathrm{d}\theta = 0, \tag{4.12}$$

which, when discretized, yields an expression for $\psi_{0,j,l}$ in terms of $\psi_{i,j,l}$ and $\zeta_{i,j,l}$, $i = 1, 2$.

At each time step an iteration procedure is adopted to obtain a converged solution. For the stream function over-relaxation accelerates convergence with a relaxation factor, typically, 1.2 whilst for the vorticity under-relaxation is necessary with a relaxation factor 0.5 for boundary points and, typically, 0.8 elsewhere. The iteration procedure is carried out until both

$$\sum \left| 1 - \frac{\zeta_{i,j,l}^{k_i}}{\zeta_{i,j,l}^{k_i - 1}} \right| < \sigma, \qquad |I_{2\pi}| < \sigma, \tag{4.13}$$

where summation extends over all the mesh points, k_i is an iteration count and σ a pre-assigned tolerance which is taken as 10^{-4} for all the results that we present.

From the converged solution the lift L, and drag D, on the cylinder may be determined from which we define lift and drag coefficients as

$$C_L = \frac{L}{\rho U_0^2 a} = \frac{L}{\rho a^3 \omega^2}, \quad C_D = \frac{D}{\rho U_0^2 a} = \frac{D}{\rho a^3 \omega^2}. \tag{4.14}$$

Each of these force coefficients includes contributions from both shear and normal stresses, and are determined as

$$C_L = \frac{1}{R_b}\int_0^{2\pi} \zeta_{r=1} \cos\theta \mathrm{d}\theta - \int_0^{2\pi} p_{r=1} \sin\theta \mathrm{d}\theta, \tag{4.15}$$

$$C_D = -\frac{1}{R_b}\int_0^{2\pi} \zeta_{r=1} \sin\theta \mathrm{d}\theta - \int_0^{2\pi} p_{r=1} \cos\theta \mathrm{d}\theta, \tag{4.16}$$

where $p = p'/\rho U_0^2 = p'/\rho a^2 \omega^2$. We note, from the θ-momentum equation, that

$$\frac{\partial p}{\partial \theta} = \frac{1}{R_b}\left(\frac{\partial \zeta}{\partial r}\right)_{r=1} \tag{4.17}$$

and so, integrating the second term in each of (4.15), (4.16) by parts and using (4.17) yields

$$C_L = -\frac{1}{R_b}\int_0^{2\pi} \left\{\frac{\partial}{\partial r}\left(\frac{\zeta}{r}\right)\right\}_{r=1} \cos\theta \mathrm{d}\theta, \tag{4.18}$$

$$C_D = \frac{1}{R_b}\int_0^{2\pi} \left\{\frac{\partial}{\partial r}\left(\frac{\zeta}{r}\right)\right\}_{r=1} \sin\theta \mathrm{d}\theta. \tag{4.19}$$

5. Perturbation solution $\epsilon \ll 1, R_b = O(1)$

The computational method described in §4 is independent of ϵ; the problem is characterized by the single parameter R_b. However, for the purposes for which we employ the numerical scheme, ϵ is indirectly involved in the construction of the boundary conditions at the free surface and $x = x_l, x_r$. This is based on the inviscid analysis of §2 in which it is assumed $\epsilon \ll 1$. All the results we present in §7, for the numerical scheme of the full Navier–Stokes equations, are for small values of ϵ. It therefore seems appropriate to exploit the smallness of ϵ in a perturbation scheme. As we shall see, this leads to a more efficient means of calculating the time-independent part of the solution that is of particular concern to us.

With $\epsilon \ll 1$ we expand the stream function and vorticity, respectively, as

$$\psi(\boldsymbol{x}, t) = \epsilon\psi_1(\boldsymbol{x}, t) + \epsilon^2\{\psi_2^{(u)}(\boldsymbol{x}, t) + \psi^{(s)}(\boldsymbol{x})\} + O(\epsilon^3), \tag{5.1}$$

$$\zeta(\boldsymbol{x}, t) = \epsilon\zeta_1(\boldsymbol{x}, t) + \epsilon^2\{\zeta_2^{(u)}(\boldsymbol{x}, t) + \zeta^{(s)}(\boldsymbol{x})\} + O(\epsilon^3). \tag{5.2}$$

In these equations $\boldsymbol{x}$ is a position vector and the subscripts (u) and (s) emphasize the time-dependent and time-independent components of the solution at $O(\epsilon^2)$. For the domains $\Omega_{II}, \Omega_{III}$, we now substitute (5.1), (5.2) into equations (4.2), (4.3) and equate coefficients of like powers of ϵ to get:

at $O(\epsilon)$

$$\frac{\partial\zeta_1}{\partial t} = \frac{1}{R_b}\nabla^2_{x\xi}\zeta_1, \tag{5.3}$$

$$\nabla^2_{x\xi}\psi_1 = -\zeta_1; \tag{5.4}$$

at $O(\epsilon^2)$

for the time-dependent part

$$\frac{\partial\zeta_2^{(u)}}{\partial t} + \beta_1\left\{\frac{\partial(\zeta_1, \psi_1)}{\partial(x, \xi)}\right\}^{(u)} = \frac{1}{R_b}\nabla^2_{x\xi}\zeta_2^{(u)}, \tag{5.5}$$

$$\nabla^2_{x\xi}\psi_2^{(u)} = -\zeta_2^{(u)}, \tag{5.6}$$

and for the time-independent part

$$\beta_1\left\{\frac{\partial(\zeta_1, \psi_1)}{\partial(x, \xi)}\right\}^{(s)} = \frac{1}{R_b}\nabla^2_{x\xi}\zeta^{(s)}, \tag{5.7}$$

$$\nabla^2_{x\xi}\psi^{(s)} = -\zeta^{(s)}. \tag{5.8}$$

There are equations corresponding to (5.3)–(5.8) in Ω_I, derived from equations (3.7), (3.8) that we do not find necessary to reproduce here.

It is convenient to separate the variables in (5.3)–(5.6), and the corresponding equations in Ω_I, by writing

$$\left.\begin{array}{ll} \psi_1 = F_1\cos t + f_1\sin t, & \psi_2^{(u)} = F_2\cos 2t + f_2\sin 2t, \\ \zeta_1 = G_1\cos t + g_1\sin t, & \zeta_2^{(u)} = G_2\cos 2t + g_2\sin 2t, \end{array}\right\} \tag{5.9}$$

where f_i, F_i, g_i, $G_i (i = 1, 2)$ are unknown functions of either (x, ξ) in $\Omega_{II}, \Omega_{III}$ or (r, θ)

in Ω_I. Substituting (5.9) in (5.3)–(5.6), and their counterparts in Ω_I, yields

$$\nabla^2 G_1 = R_b g_1, \quad \nabla^2 g_1 = -R_b G_1, \quad \nabla^2 F_1 = -G_1, \quad \nabla^2 f_1 = -g_1, \tag{5.10}$$

$$\nabla^2 G_2 = X_G + 2R_b g_2, \quad \nabla^2 g_2 = X_g - 2R_b G_2, \quad \nabla^2 F_2 = -G_2, \quad \nabla^2 f_2 = -g_2, \tag{5.11}$$

and (5.7), (5.8) can be written as

$$\nabla^2 \zeta^{(s)} = X_s, \quad \nabla^2 \psi^{(s)} = -\zeta^{(s)}. \tag{5.12}$$

In equations (5.10)–(5.12) ∇^2 represents $\nabla^2_{x\xi}$ in Ω_{II}, Ω_{III} or $\nabla^2_{r\theta}$ in Ω_I; other quantities are defined as

$$\left.\begin{aligned} X_G &= \frac{\beta_1 R_b}{2}\left\{\frac{\partial(G_1,F_1)}{\partial(x,\xi)} - \frac{\partial(g_1,f_1)}{\partial(x,\xi)}\right\}, \\ X_g &= \frac{\beta_1 R_b}{2}\left\{\frac{\partial(G_1,f_1)}{\partial(x,\xi)} + \frac{\partial(g_1,F_1)}{\partial(x,\xi)}\right\}, \\ X_s &= \frac{\beta_1 R_b}{2}\left\{\frac{\partial(g_1,f_1)}{\partial(x,\xi)} + \frac{\partial(G_1,F_1)}{\partial(x,\xi)}\right\}, \end{aligned}\right\} \text{ in } \Omega_{II},\ \Omega_{III} \tag{5.13}$$

or

$$\left.\begin{aligned} X_G &= \frac{R_b}{2r}\left\{\frac{\partial(G_1,F_1)}{\partial(r,\theta)} - \frac{\partial(g_1,f_1)}{\partial(r,\theta)}\right\}, \\ X_g &= \frac{R_b}{2r}\left\{\frac{\partial(G_1,f_1)}{\partial(r,\theta)} + \frac{\partial(g_1,F_1)}{\partial(r,\theta)}\right\}, \\ X_s &= \frac{R_b}{2r}\left\{\frac{\partial(g_1,f_1)}{\partial(r,\theta)} + \frac{\partial(G_1,F_1)}{\partial(r,\theta)}\right\}, \end{aligned}\right\} \text{ in } \Omega_I. \tag{5.14}$$

The boundary conditions to be satisfied by equations (5.10)–(5.12) are as follows:

$$\left.\begin{aligned} &F_i = \psi_{i1}, \quad f_i = \psi_{i2}, \quad \psi^{(s)} = \psi_{20}, \\ &G_i = g_i = 0 \quad (i = 1,2), \quad \zeta^{(s)} = 0, \end{aligned}\right\} \quad \begin{aligned} &\text{on } x = x_l,\ x_r, \quad 2y_b - h_\xi \leqslant \xi \leqslant h, \\ &\text{and at } \xi = h, \quad x_l \leqslant x \leqslant x_r, \end{aligned} \tag{5.15}$$

$$F_i = f_i = G_i = g_i = \psi^{(s)} = \zeta^{(s)} = 0 \quad (i = 1,2), \quad \text{at } \xi = 2y_b - h_\xi, \quad x_l \leqslant x \leqslant x_r. \tag{5.16}$$

In addition we again require conditions for the stream function, and the vorticity, at the cylinder surface $r = 1$. As in our earlier discussion, § 4, the value of each term in the expansion for ψ in (5.1), at $r = 1$, must be determined to ensure that the pressure remains single-valued. As a consequence each term must satisfy the integral constraint (4.12) from which the value of each, at the boundary, is determined. Similarly, our earlier representation (4.11) for the boundary vorticity must be satisfied by each term in the expression (5.2).

Equations (5.10)–(5.12), to be solved subject to (5.15), (5.16) and appropriate conditions at $r = 1$, are discretized using a central-difference scheme and the resulting finite-difference equations solved numerically by a point relaxation technique similar to that outlined in § 4.

With the solution so obtained we have the force coefficients C_L, C_D given by

$$C_L = \epsilon(C_{L11}\cos t + C_{L12}\sin t) + \epsilon^2(C_{L21}\cos 2t + C_{L22}\sin 2t + C_{L20}) + ..., \tag{5.17}$$

$$C_D = \epsilon(C_{D11}\cos t + C_{D12}\sin t) + \epsilon^2(C_{D21}\cos 2t + C_{D22}\sin 2t + C_{D20}) + ... \tag{5.18}$$

Each of the coefficients of the time-harmonic terms in these expressions may be expressed, through $G_i, g_i (i = 1, 2)$, $\zeta^{(s)}$ as in (4.18), (4.19). For example

$$C_{L20} = -\frac{1}{R_b}\int_0^{2\pi}\left\{\frac{\partial}{\partial r}\left(\frac{\zeta^{(s)}}{r}\right)\right\}_{r=1}\cos\theta \mathrm{d}\theta, \tag{5.19}$$

$$C_{D20} = \frac{1}{R_b}\int_0^{2\pi}\left\{\frac{\partial}{\partial r}\left(\frac{\zeta^{(s)}}{r}\right)\right\}_{r=1}\sin\theta \mathrm{d}\theta. \tag{5.20}$$

In § 7 we compare results obtained by the perturbation method with those of the full equations for small ϵ. Both approaches are, in principle, appropriate for all finite values of R_b. However, there are numerical constraints associated with the development of a boundary layer, thickness $O(R_b^{-1/2})$, at the cylinder surface $r = 1$. This is the familiar Stokes shear-wave layer. For the mesh sizes that we have been able to employ this Stokes layer may be satisfactorily resolved up to values of $R_b = O(10^2)$. A detailed discussion of the Stokes layer, for $R_b \gg 1$, that is relevant to the present investigation, has been given by Yan & Riley (1996).

6. Perturbation solution $\epsilon \ll 1$, $R_b = O(\epsilon^{-2})$

As we have remarked above the numerical processes we have introduced, with the mesh sizes available, cannot adequately resolve the thin boundary layer that forms on the cylinder for values of R_b in excess of $O(10^2)$. In this section we are concerned with situations for which $R_b \gg 1$. We do not present details of the Stokes-layer structure, which is dealt with in detail by Yan & Riley (1996). Except we note that, as in other oscillatory flow situations, a steady tangential streaming motion persists at the edge of the Stokes layer which is shown by Yan & Riley to be determined as

$$v_s(\theta) = \frac{3}{4}\left\{\frac{\partial\psi_{11}}{\partial r}\frac{\partial^2}{\partial r\partial\theta}(\psi_{11} - \psi_{12}) + \frac{\partial\psi_{12}}{\partial r}\frac{\partial^2}{\partial r\partial\theta}(\psi_{11} + \psi_{12})\right\}_{r=1}, \tag{6.1}$$

with ψ_{11}, ψ_{12} as in (2.14).

We now concentrate specifically on the induced steady streaming, often referred to as 'acoustic' streaming, outside the Stokes layer. Our choice $R_b = O(\epsilon^{-2})$, or $R_s = \epsilon^2 R_b = O(1)$ is motivated by the fact that R_s is the appropriate Reynolds number for the streaming motion, as identified by Stuart (1963).

Again, we expand the stream function and vorticity as in (5.1), (5.2), and substitute into the Navier–Stokes equations, in a manner discussed in some detail by Yan & Riley (1996). It is the coefficient of ϵ^4 that yields the governing equations for the streaming at $O(\epsilon^2)$ as, in the subdomain Ω_I,

$$\frac{1}{R_s}\nabla^2\zeta^{(s)} = \frac{1}{r}\frac{\partial(\zeta^{(s)}, \psi^{(s)})}{\partial(r, \theta)} + V_r^d\frac{\partial\zeta^{(s)}}{\partial r} + \frac{V_\theta^d}{r}\frac{\partial\zeta^{(s)}}{\partial\theta}, \tag{6.2}$$

$$\nabla^2\psi^{(s)} = -\zeta^{(s)}, \tag{6.3}$$

where V_r^d, V_θ^d are the r- and θ-components of the Stokes drift velocity defined as

$$\boldsymbol{V}^d = \left\langle\left(\int^t \boldsymbol{v}_1 \mathrm{d}t \cdot \nabla\right)\boldsymbol{v}_1\right\rangle, \tag{6.4}$$

with $\boldsymbol{v}_1$ determined from the first-order inviscid solution of § 2 as

$$\boldsymbol{v}_1 = \left\{ \frac{1}{r}\frac{\partial}{\partial\theta}(\psi_{11}\cos t + \psi_{12}\sin t), -\frac{\partial}{\partial r}(\psi_{11}\cos t + \psi_{12}\sin t) \right\}, \tag{6.5}$$

and $\langle\cdot\rangle$ denoting a time average.

Equation (6.2) represents a balance between diffusion and convection of the time-averaged vorticity, with convection effected by the mean Lagrangian, rather than Eulerian, velocity. It is the boundary-layer version of (6.2), (6.3) that is derived by Yan & Riley (1996). Equations (6.2), (6.3) have their counterparts in the (x, ξ) coordinate system in Ω_{II}, Ω_{III}. The boundary conditions to be satisfied are

$$\psi^{(s)} = \psi_{20}, \quad \zeta^{(s)} = 0, \quad \text{at } \xi = h, \ x_l \leqslant x \leqslant x_r, \quad \text{and on } x = x_l, \ x_r, \ 2y_b - h_\xi \leqslant \xi \leqslant h, \tag{6.6}$$

$$\psi^{(s)} = 0, \quad \zeta^{(s)} = 0, \quad \text{at } \xi = 2y_b - h_\xi, \quad x_l \leqslant x \leqslant x_r. \tag{6.7}$$

There are further conditions to satisfy to ensure that our outer solution for $\psi^{(s)}, \zeta^{(s)}$ matches with the Stokes-layer solution. As far as the outer solution is concerned these are to be applied at $r = 1$. Consider first the vorticity. If $\psi^{(s)}_{i,j}, \zeta^{(s)}_{i,j}$ represent values at $r = 1 + ih_r$ $(i = 0, 1, 2, ..., M_r)$, and $\theta = jh_\theta$ $(j = 1, 2, ..., N_\theta)$ then we determine $\zeta^{(s)}_{0,j}$ as

$$\zeta^{(s)}_{0,j} = \frac{48\psi^{(s)}_{1,j} - 3\psi^{(s)}_{2,j} - 45\psi^{(s)}_{0,j} + 2h_r^2(4\zeta^{(s)}_{1,j} - \zeta^{(s)}_{2,j}) + 6h_r v_{sj}(7 - 3h_r) + 4h_r^3\left(2v_s - \dfrac{\partial^2 v_s}{\partial\theta^2}\right)_j}{4h_r^2(h_r - 3)}. \tag{6.8}$$

Note when comparing (6.8) with (4.11) the role played by the streaming velocity $v_s(\theta)$ at the edge of the Stokes layer, which for the outer solution is interpreted as a velocity of slip at $r = 1$.

For the value of the stream function at $r = 1$ we again must ensure that the pressure is single-valued. To derive the condition on $\psi^{(s)}$ that ensures this we again use the θ-momentum equation and pursue our perturbation procedure. As with the stream function and vorticity we expand the velocity and pressure as

$$(\boldsymbol{v}, p) = \sum_{n=1} \epsilon^n (\boldsymbol{v}_n, p_n) \tag{6.9}$$

and substitute into the θ-momentum equation. We do not include the considerable detail of this process. It suffices to note that, again at $O(\epsilon^4)$ and following a time average,

$$\begin{aligned} \langle p_4|_{\theta=2\pi} - p_4|_{\theta=0}\rangle &= -\frac{1}{R_s}\int_0^{2\pi}\left(\frac{\partial^3\psi^{(s)}}{\partial r^3} + \frac{\partial^2\psi^{(s)}}{\partial r^2} + v_s\right)_{r=1} \mathrm{d}\theta \\ &= \frac{1}{R_s}\int_0^{2\pi}\left(\frac{\partial\zeta^{(s)}}{\partial r}\right)_{r=1} \mathrm{d}\theta = 0. \end{aligned} \tag{6.10}$$

This result is identical with (4.12), and might have been anticipated since the pressure is constant across the thin Stokes shear-wave layer. As before, equation (6.10) may be used to determine the constant $\psi^{(s)}|_{r=1}$ following a suitable discretization. The method of solution follows that outlined in § 4.

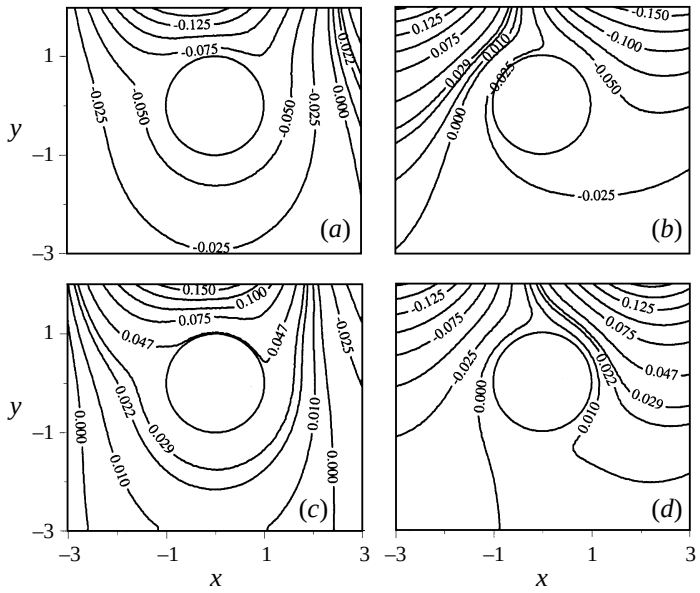

FIGURE 2. Instantaneous streamlines obtained using the full Navier–Stokes calculations with $k = 0.5, h = 2, \epsilon = 0.1$ and $R_b = 30$: (*a*) at $t - t_p = \frac{1}{2}\pi$, (*b*) at $t - t_p = \pi$, (*c*) at $t - t_p = \frac{3}{2}\pi$, (*d*) at $t - t_p = 2\pi$.

7. Results

The boundary conditions at $\xi = h$ and $x = x_l, x_r$ that we have adopted in each of § 4, § 5 and § 6 are based on the inviscid theory of § 2. The inviscid solution has been calculated using a boundary element technique; this is described in detail by Riley & Yan (1996). As we have already indicated in the introduction these boundary conditions, unlike those applied at the cylinder surface $r = 1$, are not exact. However, we may expect them to be good approximations to the exact solutions at the large Reynolds numbers and small wave amplitudes that are of interest to us. There is support for this expectation from the work of Chaplin (1984) who finds agreement, at small wave amplitudes, between the measured phase lag in the waves passing over the cylinder and the linear theory of Ogilvie (1963). Furthermore Chaplin (private communication) has recently made wave profile measurements in the nonlinear regime, and when the wave amplitude is sufficiently small so that the wave does not break as it passes over the cylinder finds excellent agreement with the inviscid results of Riley & Yan (1996).

All three approaches to the viscous problem result in the numerical solution of a system of partial differential equations. The hybrid mesh structure used, in all cases, is described in § 3. For the full unsteady Navier–Stokes calculations of § 4 a fully implicit Crank–Nicolson scheme is adopted, which has second-order accuracy and is numerically stable. The solution is marched forward in time until it is sensibly periodic. The initial conditions for ψ, ζ are arbitrary, but we calculate them in a way such that the term $\partial\zeta/\partial t$ in (3.3) is zero. Usually 30 to 40 complete periods elapse before a periodic state is achieved, which represents a considerable computational effort. The equations to be solved for the perturbation methods discussed in §§ 5 and 6 are independent of t; central differences are used for their discretization. In all cases solution of the finite-difference equations that result from discretization is carried out

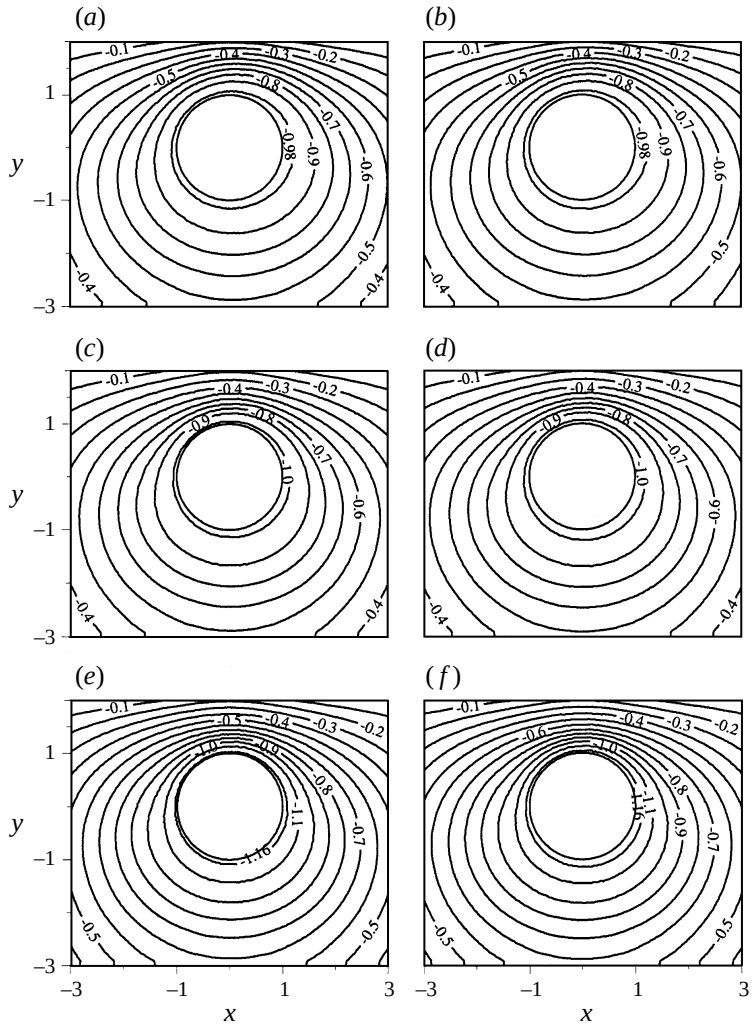

FIGURE 3. Streaming flow, $\psi^{(s)}$, for $k = 0.5, h = 2, \epsilon = 0.1$; the results shown on the left are obtained using the full Navier–Stokes equations whilst those on the right are obtained using the perturbation method in § 5: (a, b) $R_b = 30$, (c, d) $R_b = 90$, (e, f) $R_b = 150$.

using a point relaxation iteration technique. The values of x_l, x_r, r_e and y_b which set the sizes of subdomains for computational purposes vary, depending upon the value of h. For $h = 2$ we choose $x_r = -x_l = 5$ whilst for $h = 3$ we choose $x_r = -x_l = 7$; the value of r_e used in the calculations is $h - 0.2$ and in all cases $y_b = -h$. We note that in the inviscid calculation x_r and $|x_l|$ are very much larger than these values. The mesh sizes employed vary, depending upon the value of the Reynolds number. Typically, in the direction of t increasing, we have $h_t = \pi/30$ whilst in $\Omega_{II}, \Omega_{III}$ the mesh sizes in the x- and ξ-directions, h_x and h_ξ, vary from $1/20$ to $1/30$, the corresponding mesh sizes, h_r, h_θ, in the solution domain Ω_I, respectively in the range $1/50$ to $1/40$ and $\pi/80$ to $\pi/60$, are smaller since larger flow variations are anticipated close to the cylinder. We present results below for various values of the parameters involved, but in particular for variations with Reynolds number. And although our different

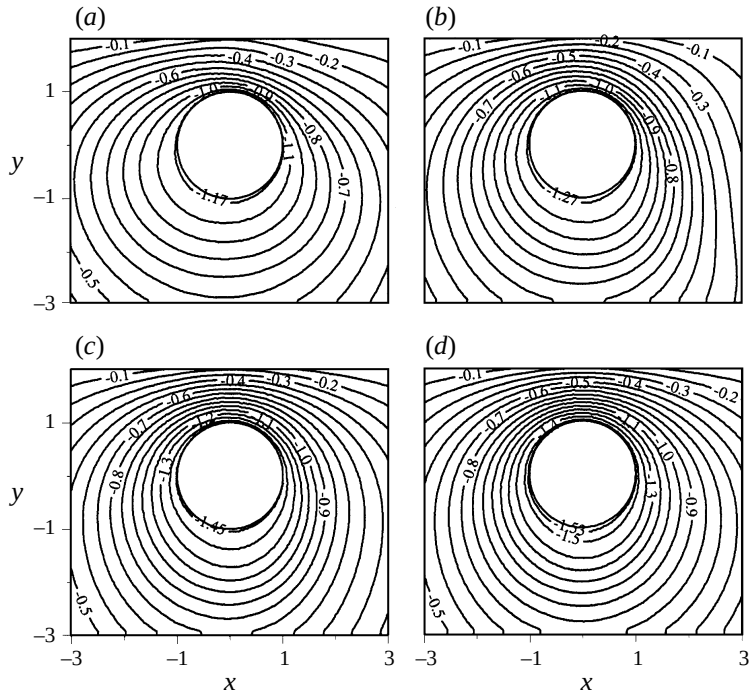

FIGURE 4. Streaming flow, $\psi^{(s)}$, for $k = 0.5, h = 2$ and (*a*) for $R_s = 1.5$, (*b*) $R_s = 20$, (*c*) $R_s = 50$, (*d*) $R_s = 100$.

approaches enable us to calculate overall flow properties up to $O(\epsilon^2)$, we do pay more attention to the time-averaged flow about the cylinder.

In figure 2 we show instantaneous streamlines as calculated from the full Navier–Stokes equations, § 4, at times $t - t_p = \pi/2, \pi, 3\pi/2, 2\pi$, where $t_p = 2n\pi$ is a time that is sufficiently large for a periodic flow to have been established. The parameter values for this case are $k = 0.5, h = 2, \epsilon = 0.1$ and $R_b = 30$. We note, in particular, that the streaming pattern at $t - t_p = 2\pi$ is not quite the mirror image about $\psi = 0$ of the streamline pattern at $t - t_p = \pi$; this is due to the presence of the streaming, or non-zero time-averaged component of the flow which is in the nature of a circulatory flow around the cylinder.

We turn next to this time-averaged component of the flow. First, we compare the results obtained from the full Navier–Stokes equations, as described in § 4, with those obtained from the perturbation solution of § 5. Both are appropriate for $R_b = O(1)$, and whereas the perturbation approach depends upon $\epsilon \ll 1$ the Navier–Stokes approach does not. However, for any comparison to be meaningful, a small value, of ϵ must be adopted in the Navier–Stokes equations, and here we take $\epsilon = 0.1$. Other parameter values are $k = 0.5, h = 2$, and we present the time-averaged streamlines in figure 3 for values of $R_b = 30, 90$ and 150. From the full Navier–Stokes solution the streaming is extracted, for $t > t_p$, by taking a time-average of the solution over a period of 2π, and dividing the result by ϵ^2. As may be expected the results obtained by the two methods are very close, but not identical for the reason that implicit within the Navier–Stokes solution are higher-order terms in ϵ that are, of course, explicitly ignored in the time-independent solution $\psi^{(s)}, \zeta^{(s)}$ of (5.1), (5.2). The computational labour involved in solving the full Navier–Stokes equations, § 4, is

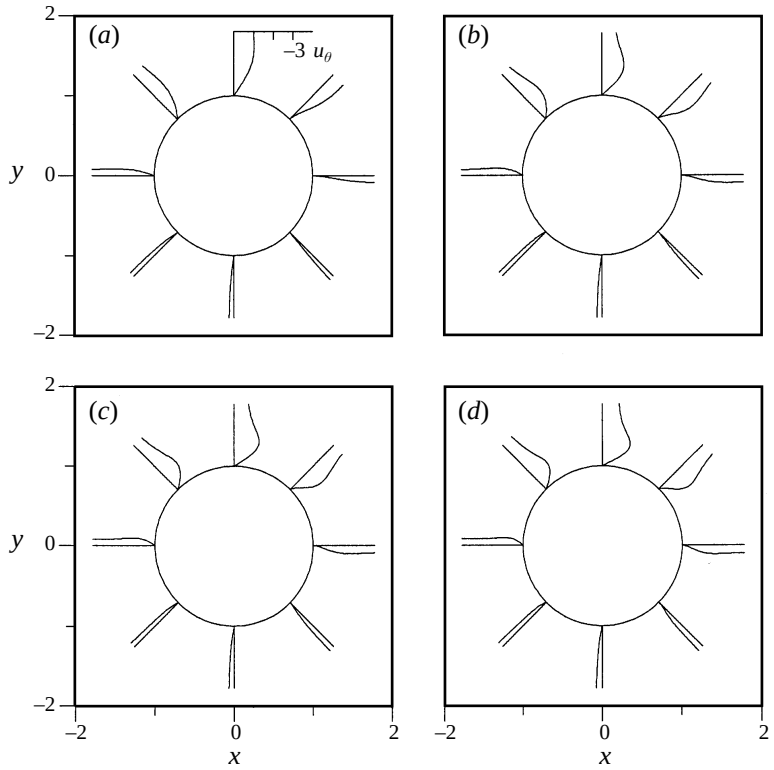

FIGURE 5. Tangential velocity distributions obtained using the perturbation method in § 5 with $k = 0.5, h = 2$: (*a*) $R_b = 30$, (*b*) $R_b = 70$, (*c*) $R_b = 110$, (*d*) $R_b = 150$.

enormous compared with that for the perturbation method, § 5. The results presented in figure 3 confirm the effectiveness of the perturbation approach which is, therefore, clearly to be preferred for values of $R_b = O(1)$. We note from figure 3 that as R_b increases so does the absolute value of the stream function at the cylinder surface. This implies an increasingly vigorous circulatory flow as the Reynolds number R_b increases.

For R_b greater than $O(10^2)$ neither of the methods of §§ 4 and 5 is appropriate on account of the development of the thin Stokes shear-wave boundary layer at the cylinder surface. The perturbation solution of § 7 for $R_s = \epsilon^2 R_b = O(1)$ is then appropriate. The Stokes layer in that case is accounted for explicitly and, with the first-order inviscid solution determined, the steady streaming beyond the Stokes layer is obtained from the solution of equations (6.2) and (6.3) and their counterparts in Ω_{II} and Ω_{III}. In figure 4 we show steady streaming streamlines $\psi^{(s)} =$ constant for $k = 0.5, h = 2$ and the range of the streaming Reynolds numbers $R_s = 1.5, 20, 50$ and 100. These flow patterns show a continuous development of those of figure 3 with, again, an increasingly vigorous circulatory flow with Reynolds number. We draw attention, in particular, to figure 4(*a*). The value $R_s = 1.5$ corresponds, with $\epsilon = 0.1$, to $R_b = R_s/\epsilon^2 = 150$. And indeed we see the close resemblance between the streaming flow patterns displayed in figures 3(*e*), 3(*f*) and 4(*a*) which demonstrates that our different approaches to this problem are in harmony. To quantify this we may usefully compare the values of $\psi^{(s)}$ at $r = 1$. For $R_b = 30, 90, 150$ these values are, from the full Navier–Stokes equations of § 4 and the perturbation approach of

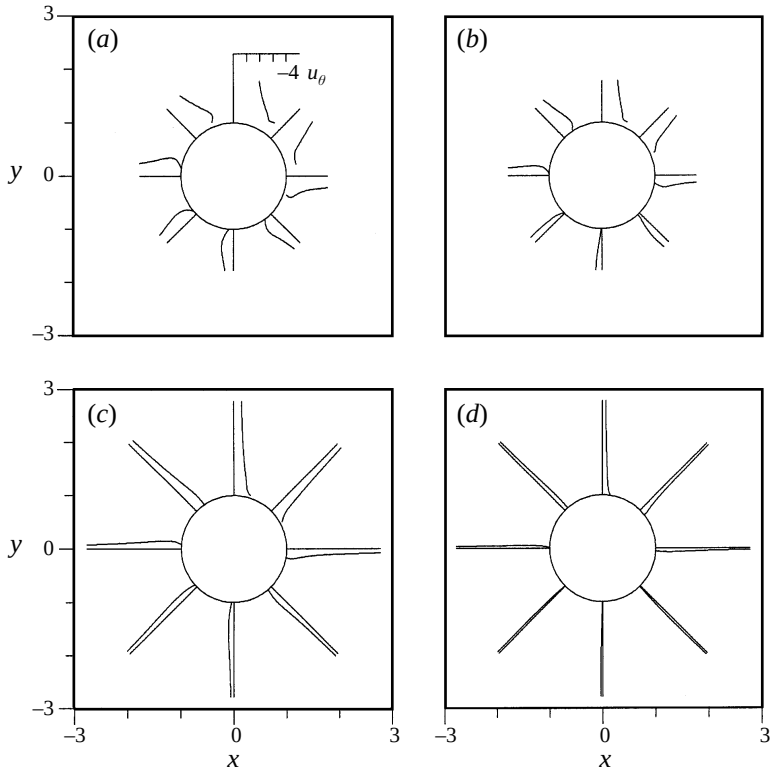

FIGURE 6. Tangential velocity distributions obtained using the streaming Navier–Stokes calculations in § 6 for $R_s = 100$: (*a*) $(k, h) = (0.3, 2)$, (*b*) $(k, h) = (0.5, 2)$, (*c*) $(k, h) = (0.3, 3)$, (*d*) $(k, h) = (0.5, 3)$.

§ 5, $(-0.988, -0.989)$, $(-1.01, -1.01)$, $(-1.16, -1.17)$. And in the latter case we have for $R_s = 1.5$, from the perturbation theory of § 6, $\psi^{(s)}|_{r=1} = -1.18$. As R_s increases the flow close to $r = 1$ assumes a boundary-layer character with a boundary layer of thickness $O(R_s^{-1/2})$ within which is embedded the Stokes layer, which is thinner by an amount $O(\epsilon)$. Outside this double boundary-layer structure the flow becomes effectively inviscid. A consequence of this is that the clockwise circulation outside the boundary layers will approach that which is predicted by Yan & Riley (1996) in their theory associated with the formal limiting process $R_s \to \infty$. Whilst the streamline patterns for the time-averaged flow give some indication of the circulatory flow about the cylinder, tangential velocity profiles are perhaps more revealing. In figure 5 we show such velocity profiles in the neighbourhood of the cylinder with $k = 0.5, h = 2$ for various values of R_b, as calculated from the perturbation solution of § 5. We note, as already anticipated, the Stokes-layer formation as R_b increases, and that the velocity magnitude is greatest over the upper part of the cylinder. In figure 6 velocity profiles are presented for the case $R_s = 100$ for various values of k and h, as calculated from the perturbation method in § 6. Similar features are noted, including the development of an outer boundary layer. We also see that the vigour of the circulatory flow increases as the cylinder depth decreases and the length of the surface waves increases. The tangential velocity at $r = 1$ in this case represents that at the edge of the Stokes layer which is, of course, non-zero.

We turn next to the circulation associated with the time-averaged flow $\psi^{(s)}$. Figure

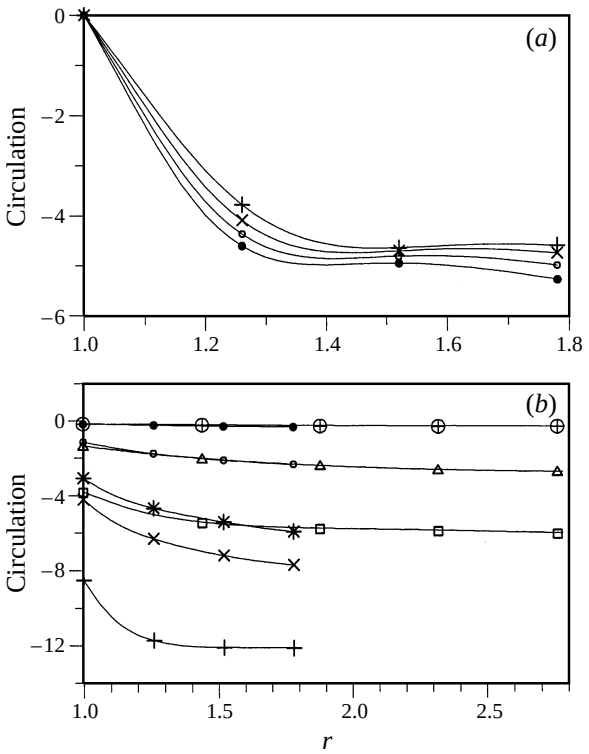

FIGURE 7. Circulations obtained for various values of k, h, R_b and R_s: (*a*) using the perturbation method in § 5 for $k = 0.5, h = 2, \epsilon = 0.1$: —+—, $R_b = 90$; —×—, $R_b = 110$; —○—, $R_b = 130$; —●—, $R_b = 150$; (*b*) using the streaming Navier–Stokes calculations in § 6 for $R_s = 100$ with various values of k and h: —+—, $k = 0.3, h = 2$; —×—, $k = 0.5, h = 2$; —*—, $k = 0.6, h = 2$; —○—, $k = 1, h = 2$; —●—, $k = 2, h = 2$; —□—, $k = 0.3, h = 3$; —△—, $k = 0.5, h = 3$; —⊕—, $k = 1, h = 3$.

7(*a*) shows the circulation, as calculated from the perturbation approach of § 5, for $k = 0.5, h = 2$ and various values of R_b, and at various radial stations. The circulation is, of course, zero at the cylinder and changes rapidly across the Stokes layer in each case to a value that, in magnitude, slightly exceeds the value 4.2 calculated by Yan & Riley (1996) at the edge of the Stokes layer. In figure 7(*b*) the circulation is shown at several radial stations when $R_s = 100$ for various values of k and h. The circulation at $r = 1$ is not zero since, in the perturbation approach in § 6, this now represents the edge of the Stokes layer. For small values of k and h there is clear evidence of the formation of an outer boundary layer; less so as the streaming velocity reduces in magnitude. It is of interest to compare the circulation outside this outer boundary layer, insofar as it can be determined from results displayed in figure 7(*b*), with those of Yan & Riley (1996), as in table 1. The analysis of Yan & Riley, which involves resolving a non-uniqueness of the inviscid flow by careful matching with the outer boundary layer at the cylinder surface, is carried out in the formal limit $R_s \to \infty$. By contrast the results presented here are for finite R_s, and as a consequence we consider the agreement, shown in table 1, to be good.

We next consider the forces acting on the cylinder. In figure 8(*a, b*) we show the time variation, over a complete period, of the lift and drag coefficients for $k = 0.5, h = 2, \epsilon = 0.1$ and various values of R_b. These results are obtained from the perturbation method of § 5, and are almost indistinguishable graphically from

	$h = 2$			$h = 3$	
Circulations	$k = 0.3$	$k = 1$	$k = 2$	$k = 0.3$	$k = 1$
Current method with $R_s = 100$	−12.1	−2.36	−0.357	−6.05	−0.361
Yan & Riley (1996)	−10.6	−2.19	−0.371	−4.76	−0.25

TABLE 1. The circulations

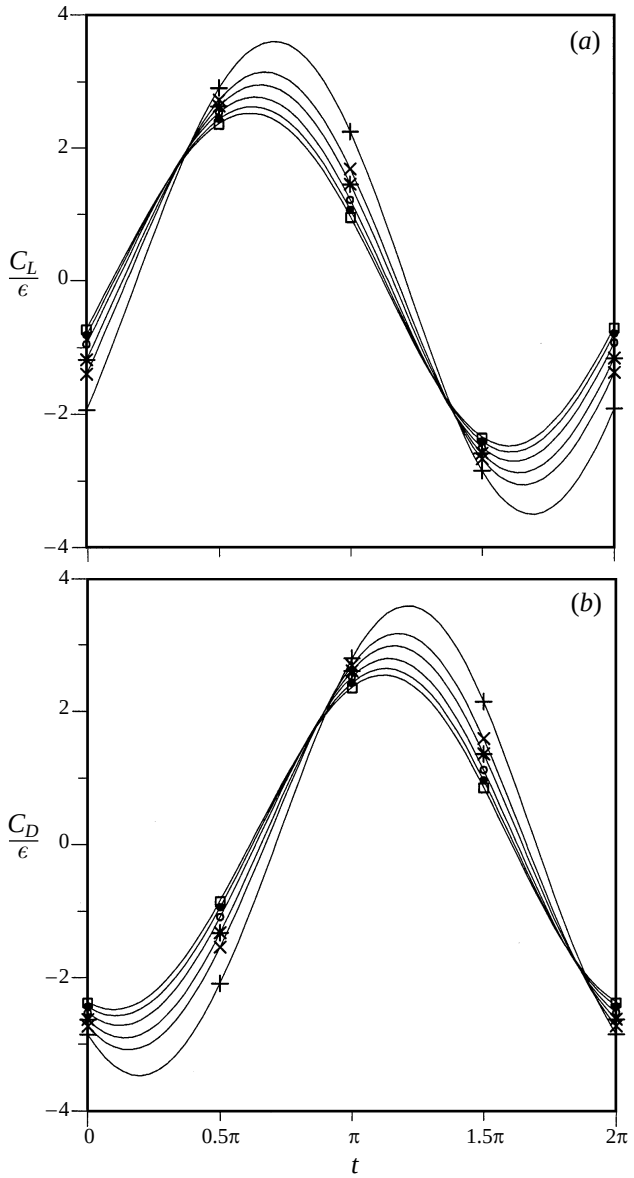

FIGURE 8. Lift and drag coefficients for $k = 0.5, h = 2, \epsilon = 0.1$ and various values of R_b, as calculated using the perturbation method in § 5: —+—, $R_b = 10$; —×—, $R_b = 20$; —*—, $R_b = 30$; —○—, $R_b = 50$; —●—, $R_b = 90$; —□—, $R_b = 150$. (*a*) Lift coefficient, (*b*) drag coefficient.

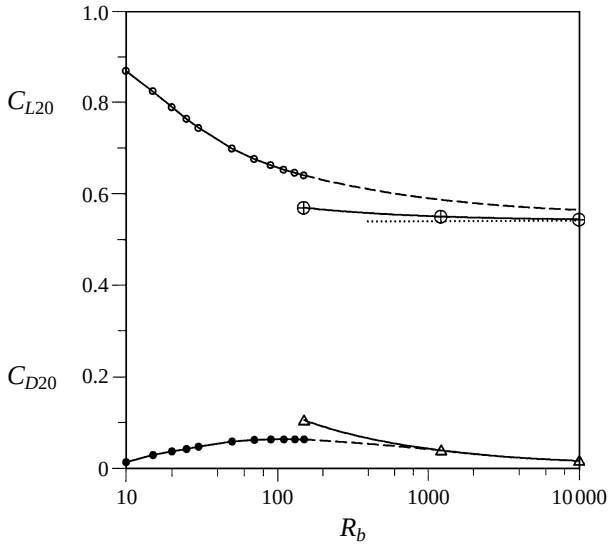

FIGURE 9. Second-order lift and drag coefficients for $k = 0.5, h = 2$: —○—, $C_{L20}, 10 \leqslant R_b \leqslant 150$; —●—, $C_{D20}, 10 \leqslant R_b \leqslant 150$; —⊕—, $C_{L20}, R_s = O(1)$; —△—, $C_{D20}, R_s = O(1)$; – – – – –, suggested extrapolation; ·····, C_{L20} as obtained from the inviscid solution of Ogilvie (1963).

those obtained from the full Navier–Stokes equations. The fluctuating lift and drag forces are comparable in order of magnitude, with the phase of the latter lagging by an amount $\pi/4$ compared with the lift. As the Reynolds number R_b increases, C_L and C_D approach limiting forms since, for the wave amplitudes considered, there is no flow separation. Although it is not immediately obvious from figure 8 the force coefficients do, as we know, have a non-zero time average. In figure 9 we present the time-independent lift and drag coefficients defined in (5.17)–(5.20). In addition to results from the perturbation theory of § 5, up to $R_b = 150$, we also include results for $R_b \gg 1$ calculated from the theory of § 6. The contribution from the pressure, since pressure is constant across the Stokes layer, is determined from $\langle p_2 \rangle$, see (6.9). The shear stress contribution is determined from the Stokes-layer solution, and is of relative order of $\epsilon/R_s^{1/2}$ or $R_b^{-1/2}$ compared to that of the pressure. From figure 9 we see that the horizontal, or drag, force tends to zero as $R_b \to \infty$ but the vertical, or lift, force tends to the finite value given by Ogilvie's (1963) inviscid solution. The persistence of lift in the infinite-Reynolds-number limit is not unexpected since in the undisturbed waves, the total acceleration in the vertical direction at a given submergence has a non-zero mean.

Chaplin (1984) has measured the forces on a cylinder beneath waves on water of depth large compared with the cylinder radius. We are able to make a comparison with some of the results for his Case E, for which $h = 2, k = 0.206, R_b = 9488$. In figure 10 we show the amplitude of the dominant lift force coefficient as a function of R_b. For $R_b \leqslant 150$ the constituent parts are calculated in a manner similar to (5.19). For larger values of R_b we use, as with the results in figure 9, the theory of § 6 with the pressure contribution now calculated from p_1 in (6.9), and the shear stress from the Stokes layer. The latter, again, is of relative order $R_b^{-1/2}$. Our results are seen to agree closely with the measured result of Chaplin at $R_b = 9488$ and to be consistent with Ogilvie's (1963) inviscid result. Finally, we make a comparison with Chaplin's

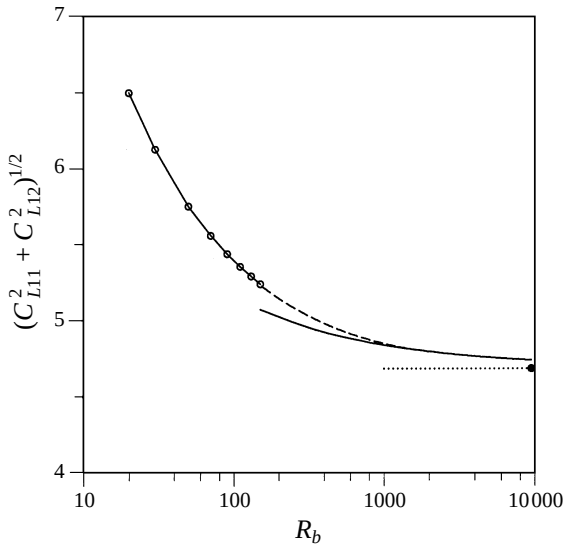

FIGURE 10. Magnitude of the first-order lift as a function of R_b for $k = 0.206, h = 2$: —o—, $20 \leqslant R_b \leqslant 150$; ———, $R_s = O(1)$; – – – – –, suggested extrapolation; •, Chaplin (1984), Case E; ·····, Ogilvie (1963).

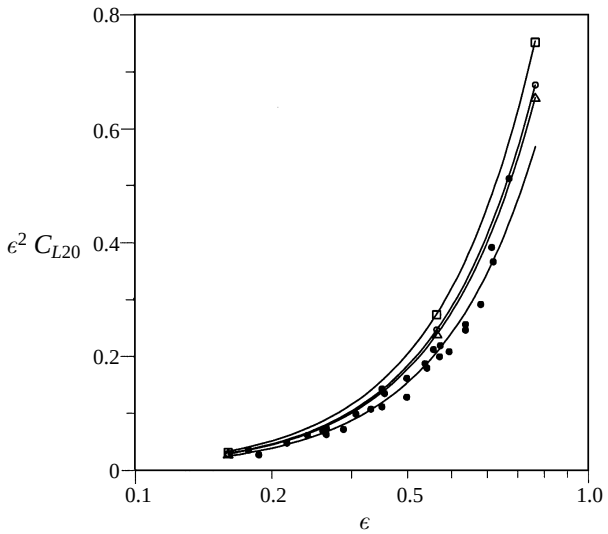

FIGURE 11. Second-order lift as a function of ϵ for $k = 0.206, h = 2$: •, Chaplin (1984), Case E; method of § 5, —□—, $R_b = 30$; —o—, $R_b = 90$; —△—, $R_b = 150$; method of § 6, ———, $R_b = 9488$.

measured, time-averaged lift as ϵ varies. The experimental results are plotted in figure 11, where we also include the lift, calculated from (5.19), from our perturbation method of § 5 for values of R_b in the range $30 \leqslant R_b \leqslant 150$. Although these Reynolds numbers are smaller by a factor $O(10^2)$ than the experimental value, we see that the results reflect the trend of the measured force, and approach the measured values as R_b increases. The experimental results encompass values of the streaming Reynolds number in the range $O(10^2)$ to $O(10^3)$, and therefore fall within the framework of § 6.

The time-averaged lift coefficient from the theoretical development for $R_s = O(1)$ is seen, in figure 11, to match the measured values very closely, except for the larger values of ϵ where terms of higher order than those we have calculated in our series (5.1), (6.9) may be expected to be non-negligible. The lift coefficient is dominated by $\langle \epsilon^2 p_2 \rangle$, and although we have included the leading-order time-independent shear stresses, determined from the Stokes layer, these are of relative order $\epsilon/R_s^{1/2}$, and contribute an insignificant amount to the results shown in figure 11. Our results offer an explanation for the good agreement, for the lift coefficient, between the viscous predictions at high Reynolds numbers and the analytical inviscid solution of Ogilvie (1963). It should be noted that some other components of the force are strongly influenced by non-zero viscosity.

8. Conclusions

For a circular cylinder placed beneath a free surface on which waves of small, dimensionless, amplitude ϵ propagate we have studied the resulting flow at finite Reynolds number. With $R_b = a^2\omega/\nu = O(1)$ we have adopted a two-pronged approach. On the one hand we have attacked the Navier–Stokes equations directly, whilst on the other we have taken advantage of the fact that $\epsilon \ll 1$ and constructed a regular perturbation series. The results from the two approaches are in excellent agreement. That being so the perturbation approach is to be preferred since, unless transient effects, following an impulsive start say, are important the direct numerical approach is far more demanding of computer time. For $R_b \gg 1$ neither approach is appropriate on account of the thin Stokes shear-wave layer that develops on the cylinder. For large Reynolds numbers we have adopted, in § 6, a singular perturbation approach. This is valid for $R_b = O(\epsilon^{-2})$, or $R_s = \epsilon^2 R_b = O(1)$. This latter parameter is known to be appropriate as the Reynolds number for the induced time-independent, or streaming, component of the flow. In this formulation the Stokes layer is accounted for explicitly, and the solution for the flow outside it addressed directly. For R_s small we are able to demonstrate agreement with the results obtained from the formulation for $R_b = O(1)$. Similarly, for $R_s \gg 1$, we are able to demonstrate that the solutions are approaching those of Yan & Riley (1996), where the formal limit $R_s \to \infty$ resulted in a double boundary-layer structure at the cylinder surface.

For waves of small amplitude the fluid flow of the title problem, correct to $O(\epsilon^2)$, has been treated in the inviscid flow limit by Riley & Yan (1996), and in the infinite Reynolds number limit for a viscous fluid by Yan & Riley (1996). In the present paper we have endeavoured to extend these results to finite Reynolds numbers. Since viscous effects will be largely confined to the region of the cylinder itself, at which the no-slip condition must be satisfied, we have approximated the free-surface conditions by adopting values of the stream function at the free surface determined from the inviscid solution. We anticipate that this approximation will be a good one at the large Reynolds numbers of interest, and comparison with experiment adds confidence to this view.

The authors would like to thank the Marine Technology Directorate for financial support, and also two referees whose penetrating comments have improved this paper.

REFERENCES

Chaplin, J. R. 1984 Nonlinear forces on a horizontal cylinder beneath waves. *J. Fluid Mech.* **147**, 449–464.

Chaplin, J. R. & Retzler, C. H. 1997 Orbital flow about a submerged cylinder. Final Report on EPSRC Research Grant GR/J54031: OFF 135.

Dean, W. R. 1948 On the reflexion of surface waves by a submerged circular cylinder. *Proc. Camb. Phil. Soc.* **44**, 483–491.

McIver, M. & McIver, P. 1990 Second-order wave diffraction by a submerged circular cylinder. *J. Fluid Mech.* **219**, 519–529.

Ogilvie, T. F. 1963 First- and second-order forces on a cylinder submerged under a free surface. *J. Fluid Mech.* **16**, 451–472.

Riley, N. & Yan, B. 1996 Inviscid fluid flow around a submerged circular cylinder induced by free-surface travelling waves. *J. Engrg Maths* **30**, 587–601.

Stuart, J. T. 1963 Unsteady boundary layers. In *Laminar Boundary Layers*. Oxford University Press.

Ursell, F. 1950 Surface waves on deep water in the presence of a submerged circular cylinder. I. *Proc. Camb. Phil. Soc.* **46**, 141–152.

Vada, T. A. 1987 A numerical solution of the second-order wave-diffraction problem for a submerged cylinder of arbitrary shape. *J. Fluid Mech.* **174**, 23–37.

Woods, L. C. 1954 A note on the numerical solution of fourth order differential equations. *Aero. Q.* **5**, 176–184.

Wu, G. X. 1991 On the second order wave reflection and transmission by a horizontal cylinder. *Appl. Ocean Res.* **13**, 58–62.

Yan, B. & Riley, N. 1996 Boundary-layer flow around a submerged circular cylinder induced by free-surface travelling waves. *J. Fluid Mech.* **316**, 241–257.